BURST PRESSURE PREDICTIONS OF CORRODED PIPELINES WITH LONG DEFECT

Mario S. G. Chiodo, mario.chiodo@poli.usp.br
Claudio Ruggieri, claudio.ruggieri@usp.br
Department of Naval Architecture and Ocean Engineering, PNV-EPUSP
University of São Paulo, São Paulo, SP 05508−900, Brazil

Abstract. This study examines the applicability of a stress-based criterion based upon plastic instability analysis to predict the failure pressure of corroded pipelines with axial defects. A central focus is to gain additional insight into effects of defect geometry and material properties on the attainment of a local limit load to support the use of stress-based burst strength criteria. The presentation begins with a parametric study conducted on plane-strain models for a flawed pipe containing an axial defect with varying geometry and material flow properties. These analyses provide an extensive body of results which lend further support to adopt failure criteria for corroded pipelines based upon ligament instability analyses. Verification analyses conducted on burst testing of large-diameter pipe specimens with varying defect configuration made of API X65 and X100 steels show the effectiveness of a stress-based criterion in burst pressure predictions, even though the η -factor exhibits a potential dependence on defect geometry and possibly on material's strain hardening capacity. Overall, the results presented here suggest that use of stress-based criteria based upon plastic instability analysis of the defect ligament is a valid engineering tool for integrity assessments of pipelines with axial corroded defects.

Keywords: burst pressure, corrosion defects, failure criteria, pipeline, limit load

1. INTRODUCTION

Accurate evaluation of the residual strength for corroded pipes remains essential in fitness for service analyses, including repair decisions and life-extension programs, of onshore and offshore oil and gas transportation. As the pipeline infrastructure ages, the loss of material due corrosion represents one of the main degradation factors of steel pipes which leads to severe strength reduction and potential catastrophic failures (Eiber and Kiefner, 1986). While current high resolution methods are now able to precisely measure the geometry of corrosion defects, they are still insufficient to ensure high levels of reliability in burst pressure assessments and specification of critical defect sizes for in-service piping systems.

Current codes and standards to assess the integrity of corroded pipes, such as ASME B31.G (ASME, 1991), RSTRENG (Kiefner e Vieth, 1989), DNV RP-F101 (DNV, 2004), among others, provide simplified acceptance criteria based on a limit load solution for pressurized cylinders with longitudinal crack-like-flaws or defects. Although these widely used criteria clearly simplify integrity assessments of in-service pipe components, they essentially derive from semi-empirical analyses based on thin wall cylindrical specimens made of low to moderate strength steels (e.g., API X52 and X60) with machined defects.

It became evident in the last few years that conventional fitness-for-service procedures for corroded pipes are quite limited for burst pressure assessments of damaged equipments and pipelines. Most often, these procedures provide overly conservative and pessimistic analyses. Although such high levels of conservatism ensure additional safety, it can also lead to cost elevation due to unnecessary repairs and replacement of in-service pipeline sections. Moreover, the failure equations incorporated in current codes do not address specific requirements for high grade steels. Indeed, high strength steels (e.g., API X100 and X120) used in high pressure pipelines exhibit lower strain hardening capability and lower strain to failure than low to moderate strength pipeline steels (e.g., API X60 and X70). Such features may have an important influence in failure predictions of damaged pipes made of high grade materials when using conventional procedures. Recent exploratory studies (Maes et al., 2006) suggest that an API X100 steel pipe may be less tolerant to defects than lower grade steel pipes, such as an API X60.

The previous observations motivated further developments in conventional assessment methodologies for corrosion defects. These developments evolved primarily along the use of analyses based on stress-based criteria (Fu et al., 1995, Karstensen et al., 2001, Noronha et al., 2002, Choi et al., 2003). Here, failure occurs when the equivalent stress (such as von Mises) over the remaining defect ligament reaches a reference stress, σ_{ref} , which is defined as a fraction of the ultimate tensile stress, σ_u , i.e., $\sigma_{ref} = \eta \sigma_u$, where η often ranges from 0.8 to 1.0. These research efforts proved effective to generate more accurate failure prediction of pipelines removed from service. However, while these studies report agreement between predicted and experimentally measured burst pressures with ±10% deviation, the η factor adopted to specify the reference stress appears to be dependent on defect configuration and material properties. Indeed, previous analyses conducted by Choi et al. (2003) suggest the utilization of $\eta = 0.9$ for rectangular defects and $\eta = 0.8$ for elliptic defects. Failure criteria to be used in defect assessment should provide integrity analyses independent of

such factors. Consequently, development of robust methods for structural integrity analyses become central to specifying critical defect sizes which enter directly into procedures for corroded piping components.

As a step in this direction, this work addresses the applicability of a stress based criterion based upon plastic instability of defect ligament to predict the burst pressure of oil and gas pipelines with axial corrosion defects. A central focus is to gain a new understanding of defect geometry and material properties effects on the attainment of a local limit load to support the development of a stress based criterion. The presentation begins with a parametric study conducted on plane-strain models for a flawed pipe containing an axial defect with varying geometry and material flow properties. These analyses provide an extensive body of results which lend further support to adopt failure criteria for corroded pipelines based upon ligament instability analyses. Verification studies based on experimental burst tests of large diameter pipes made of API X65 and X100 steels with different defect length showed the effectiveness of the proposed criterion based on $\sigma_{ref} = \eta \sigma_u$ in failure predictions, even though the η factor exhibits a potential strong dependence on defect geometry and material properties. In general, the results presented here lend further support of the proposed stress based criterion based upon plastic instability of the remaining ligament in integrity assessments of pipelines with longitudinal corrosion defects.

2. NUMERICAL PROCEDURES AND COMPUTATIONAL MODELS

2.1. Parametric Studies of Flawed Pipes

Nonlinear finite element analyses are described for plane-strain models of axially flawed pipes with $D = 508 \, mm \, (20 \, pol)$, $t = 15 \, mm \, (D/t = 34)$ and external surface defects having $a/t = 0,2$ (shallow defect) and $a/t = 0,5$ (deep defect). Here, a is the crack depth, t is the pipe wall thickness and D is the pipe outside diameter. These configurations typify common geometries and flaw sizes in high pressure, high strength pipelines. To verify the effect of flaw shape and flaw width on corrosion defect assessments incorporating stress-based criteria, the matrix analysis considers groove-shaped defects with groove width, $d_g = 0.2, 0.5, 1, 3$ and 6 mm, and rectangular-shaped defects with defect width, $w_c = 25; 50; 75; 100$ and 200 mm. Figure 1 illustrates the flaw geometry adopted in the analyses.

Figure 1(a-c) also shows the finite element models constructed for the pipe configurations having $a/t = 0,2$ with $d_g = 3$ mm (groove shape) and $w_c = 25$ mm (rectangular shape). Symmetry conditions permit modeling of only one-half of the analyzed pipes. Square elements of uniform size are defined in the defect region and along the remaining ligament to provide similar levels of mesh refinement for all numerical models. Because no strong stress gradients arise in the defect region (which contrasts to conventional crack-tip problems – see, for example, Cravero et al. (2005) and Silva et al. (2006) for illustrative analyses), the evolving stresses ahead of ligament with increased pressure are resolved adequately for element sizes of $\approx 0.1 \sim 0.5$ mm. The half-symmetric model has one thickness layer of 1770 8-node, 3-D elements (3970 nodes) with plane-strain constraints ($w = 0$) imposed on each node. Very similar finite element models and mesh details are employed for other pipe configurations.

2.2. Numerical Models of API X65 and API X100 Pipes with Axial Surface Defects

Nonlinear finite element analyses were conducted on numerical models of API 5L X65 steel pipes with external diameter $D = 762$ mm (30 in) and wall thickness $t = 17.5$ mm ($D/t = 44$). Kim et al. (2004) performed hydrostatic tests on end capped specimens with length $L = 2.3$ m to experimentally measure the burst pressure. Rectangular defects with different sizes were machined on the pipe outside surface. The analysis matrix contains corroded defects with fixed depth, $a = 8.75$ mm, and (circumferential) width, $w_c = 50$ mm, and different lengths, $2c = 50, 100, 200, 300, 600$ and 900 mm.

Figure 2 shows the finite element model applied in the 3-D analysis of a specimen with defect length $2c = 900$ mm. Due to symmetry conditions only a quarter of the specimen was modeled and appropriate displacement restrictions were imposed. The quarter-symmetric model has approximately 90000 hexahedral elements (8 nodes), arranged in several variable thickness layers over the pipe half length ($L/2$), as illustrated in Figure 2(a), to accommodate potential stress gradients in the defect region, particularly at the edges. Although the machined defects have rounded edges with a 5mm radius (Kim et al., 2004), the 3-D analyzed models have square edges to simplify mesh construction. Because of the low stress gradient in the defect region, the development of stresses at the ligament region is not influenced by these mesh details. Indeed, numerical analyses to assess the suitability of the mesh refinement showed similar burst pressure with and without rounded edges. In order to simulate the experimental end-capped conditions, coupled with internal pressure, axial loads over the pipe end were applied.
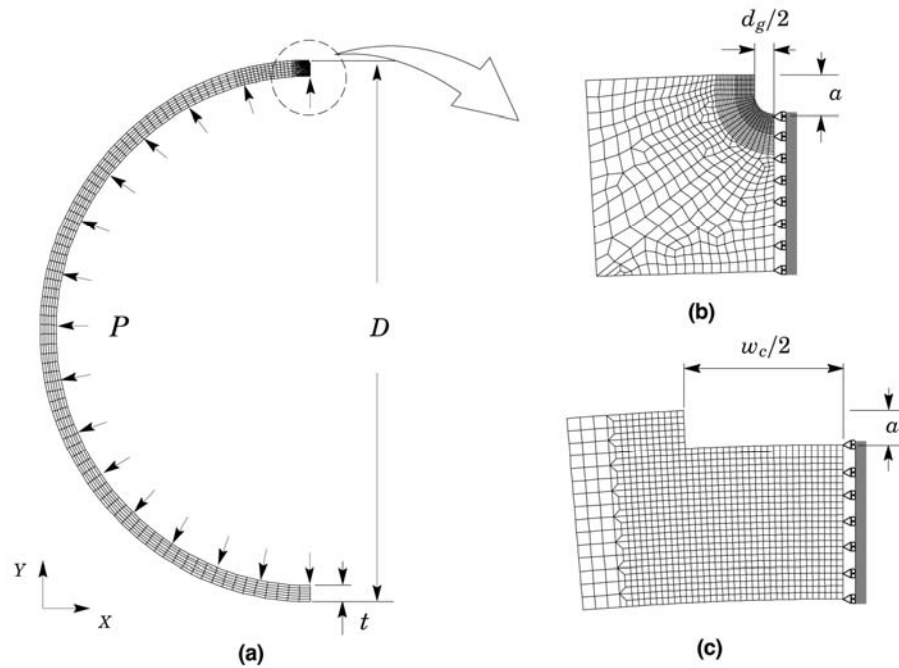
Figure 1. (a) Plane-strain finite element model for the analyzed pipe with $a/t = 0.2$; (b) Mesh detail for the groove-shaped defect; (c) Mesh detail for the rectangular-shaped defect.

.

3-D finite element analyses were also conducted on high strength, low hardening pipe specimens. Mannucci et al. (2001) recently reported on full-scale burst tests at room temperature conducted on large diameter pipes with axial surface defects made of API X100 pipeline steel. The burst tests include end-capped pipe specimens with two outside diameters: (1) $D = 914$ mm (36 in) and wall thickness, $t = 16$ mm ($D/t = 57$) with $2c = 150 \times a = 9$ mm and $2c = 450 \times a = 6$ mm; (2) $D = 1422$ mm (56 in) and wall thickness, $t = 19.1$ mm ($D/t = 74$) with $2c = 180 \times a = 10.4$ mm. Figure 3 shows the finite element model for the 3-D analysis of the pipe specimen with $D = 914$ mm (36 in) and $2c = 150 \times a = 9$ mm. The general mesh construction follows closely the previous finite element models for the X65 pipes. The quarter-symmetric model has approximately 26000 hexahedral elements (8 nodes), arranged in several variable thickness layers over the pipe half length ($L/2$), as illustrated in Figure 3(a). A groove-shaped flaw with groove width $d_g = 0.5$ mm is employed to model the axial surface defect for the pipe specimens as illustrated in Figure 3(b). As it will be discussed in Section 3, the groove width does not affect predictions of burst pressure based upon the approach adopted in the present work.

2.3. Material Model and Numerical Procedure

The elastic-plastic material employed in the parametric analyses described in Section 3 follows a J_2 flow theory with conventional Mises plasticity in small geometry change (SGC) setting. The uniaxial true stress *vs.* logarithmic strain curve obeys a simple power-hardening model,

$$\frac{\varepsilon}{\varepsilon_0} = \frac{\overline{\sigma}}{\sigma_0} \quad \varepsilon \le \varepsilon_0; \quad \frac{\varepsilon}{\varepsilon_0} = \left(\frac{\overline{\sigma}}{\sigma_0} \right)^n \quad \varepsilon > \varepsilon_0 \tag{1}$$

where σ_0 and ε_0 are, respectively, the reference (yield) stress and strain and n is the material strain hardening exponent. The finite element analyses presented here consider material flow properties representative of common pipeline and pressure vessel steels: $n = 10$ ($E/\sigma_0 = 500$) with $E = 206$ GPa and $\nu = 0.3$. Additional details and analyses for different material flow properties can be found in Chiodo and Ruggieri (2009).
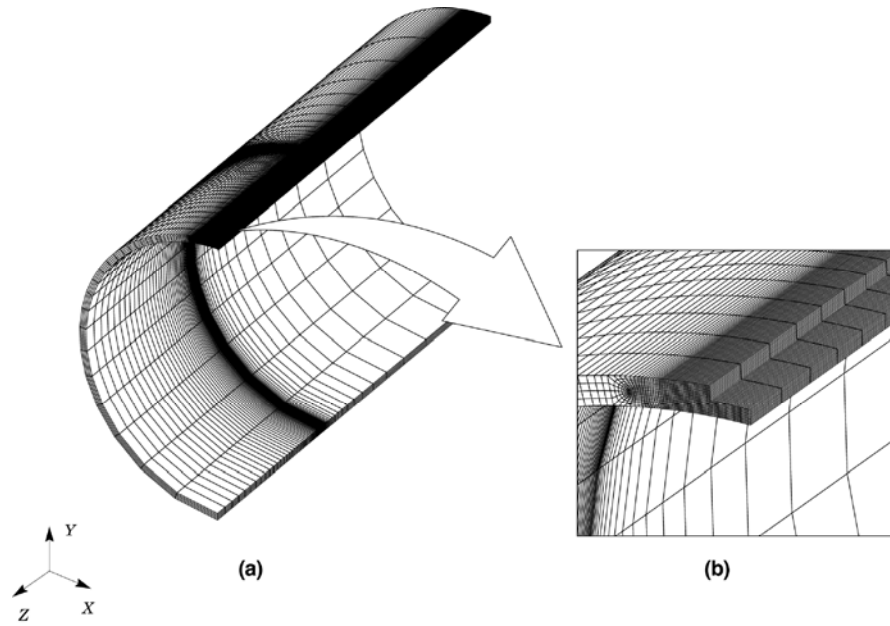
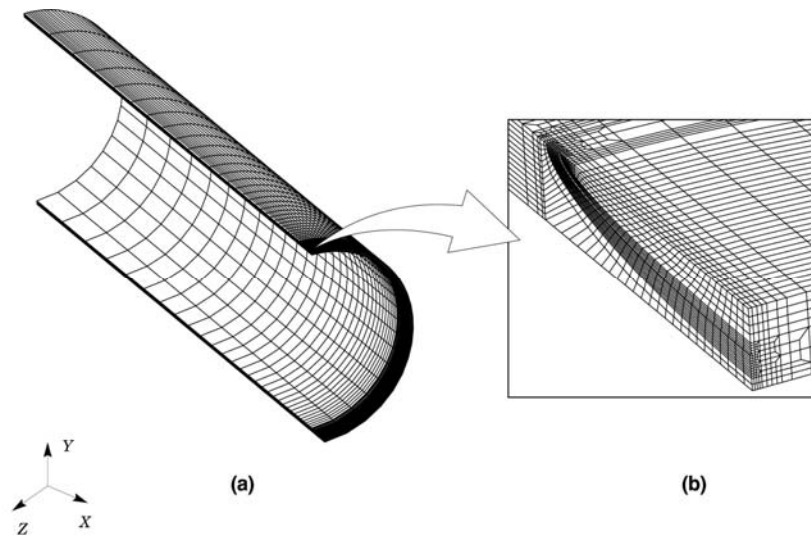**Figure 2**. 3-D finite element model for API X65 pipe specimen.

Figure 3. -D finite element model for API X100 pipe specimen.

Evaluation of plastic instability in the remaining defect ligament through the stress based criterion employed in Section 3 and 4 requires specification of the true tensile stress, σ_u, which is derived from API 579 (API, 2007)

$$\sigma_u = \sigma_{ys}\left[\frac{(500N)^N}{\exp(N)}\right] \tag{2}$$

where $N = 1/n$.

Section 4.1. describes numerical analyses of pipe specimens tested by Kim et al. (2004). The API X65 true stress-logarithmic strain behavior was modeled with a piecewise linear approximation of the experimental curve as illustrated in Figure 4. For the API X100 pipes, we adopt the tensile properties provided by Mannucci et al. (2001) to approximate the true stress-logarithmic strain response by the power hardening law given by Eq. (1) with the strain hardening exponent derived from previous Eq. (2). All these analyses also consider Young's modulus $E = 206$ GPa and Poisson's ratio $\nu = 0.3$.

All numerical models reported here were solved by the finite element code WARP3D (Koppenhoefer et al., 1994) which implements a very efficient, sparse matrix solver that significantly reduces both memory and CPU time required for solution of the linearized equations compared to conventional direct solvers. A typical analysis of the 3-D pipe models to reach ligament instability requires approximately 300 load steps solved in less than 10 hours in a SGI Itanium-based workstation.
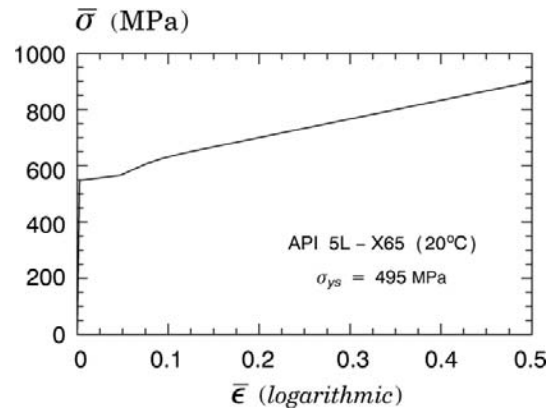

Figure 4. API X65 true stress-logarithmic strain curve (Kim et al., 2004).

3. PLASTIC INSTABILITY ANALYSES FOR PIPES WITH AXIAL DEFECTS

3.1. Fully Plastic Behavior Under Internal Pressure

Standard limit load analysis conventionally defines the global limit load (also referred to as net-section limit load) at which displacements become unbounded or unrestricted (Chakabart, 2006) thereby increasing very rapidly with little or no increase in the corresponding applied loading. Once displacements reach this point, the structure attains its maximum load-bearing capacity. When a surface crack-like flaw or a surface corrosion defect is present in the structure, the picture becomes more complex as the limit load can now be defined in terms of local instability of the remaining ligament ahead of crack or defect. The extensive finite element analyses of pipe configurations including the effects of defect shape provide additional support to define the limit load in terms of local instability of the remaining ligament ahead of defect. The central focus is to gain additional insight into effects of defect geometry (groove *vs.* rectangular) on the evolution of the highly stressed zones in the remaining defect ligament and the attainment of a local limit load.

Figures 5(a-b) display the growth of Mises stress contours corresponding to $\sigma_e \geq \sigma_u$ with increased pressure for shallow flaw pipes with groove and rectangular-shaped defects. The material properties for the analyses covered in these plots correspond to $n = 10$ and $E/\sigma_0 = 500$ which are representative of a moderately hardening material such as an API X60 ~ X70 pipeline steel.

The effect of defect shape on the spatial extent of the stress contours is amply demonstrated by comparing the results shown in these plots. For the groove-shaped flaw shown in Fig. 5(a), the Mises stress zones begin to develop at the root of the groove (which corresponds to the flaw mid-plane) and then spread across the entire ligament along an angular position of ~ 45°. It is interesting to note that the angular extension and the forward swing of the plastic lobes resemble to some extent the development of plastic zones for axially cracked pipes subjected to rather strong negative T-stress fields (see the extensive analyses and discussion provided by Cravero and Ruggieri (2005)). In contrast, a different picture emerges for the growth of stress contours for the rectangular-shaped defects shown in Fig. 5(b). Here, the Mises stress zones begin to develop at the corners of the (rectangular) defect after which they coalesce and progress across the entire ligament towards the defect mid-plane. In all analyzed cases, the plastic zones where the Mises stress exceeds the tensile stress, σ_u, spreads rapidly across the ligament with rather little increase in internal pressure.

Although not shown here in interest of space, very similar trends are also displayed for deep flaw pipes and for pipes with other material properties represented by a hardening exponent of $n = 5$ ($E/\sigma_0 = 800$) and $n = 20$ ($E/\sigma_0 = 300$).
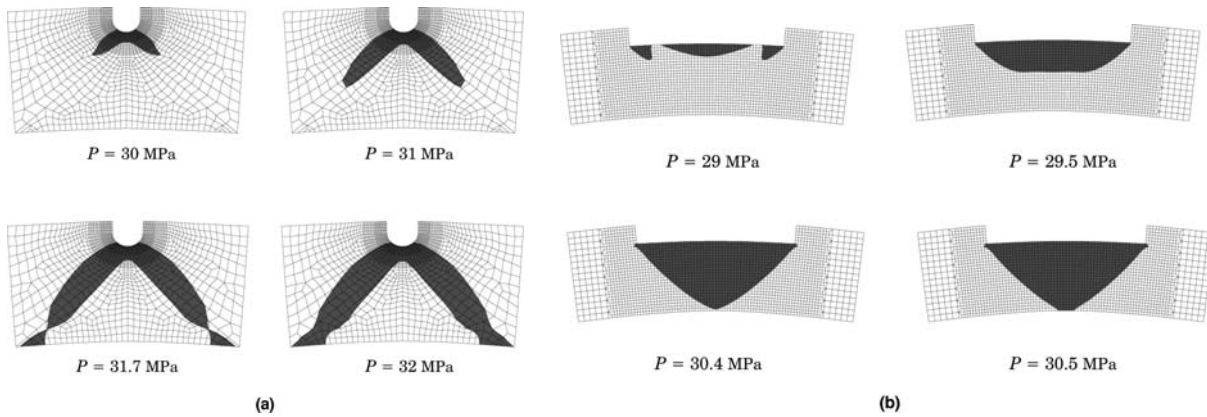
Figure 5. Mises stress contours with increased internal pressure for the shallow flaw ($a/t = 0.2$) pipe and $n = 10$, with (a) groove-shaped defect and (b) rectangular-shaped defect.

3.2. Failure Pressure for Pipes with Axial Defects

While the previous contour maps for which $\sigma_e \geq \sigma_u$ differ significantly for groove and rectangular-shaped defects, the previous results clearly provide a connection between plastic instability of the ligament and the attainment of a local limit load. Another key issue to resolve with the applicability of a stress-based criterion in burst pressure predictions of corroded pipelines lies in the effect of the growth and pattern for the evolving stress contours on the local limit load. Here, we examine the influence of defect shape and defect width on the failure pressure for the analyzed pipes.

Figures 6-7 provide the failure pressure, P_f, for shallow and deep flaw pipes with groove and rectangular-shaped defects with varying defect width. Here, the failure pressure is defined by plastic instability of the ligament as shown previously. The material properties correspond to $n = 10$ and $E/\sigma_0 = 500$. In the plots, the failure pressure is normalized by the burst pressure solution for a defect-free pipe, P_0, provided by Zhu and Leis (2005) in the form

$$P_0 = \left(\frac{C}{2}\right)^{n+1/n} \frac{4t}{D_m} \sigma_u \tag{3}$$

where C is a yield-criterion dependent constant, n is the strain hardening exponent, D_m is the average pipe diameter, t is the pipe wall thickness and σ_u is the material's true tensile strength. In the above expression, the value $C = 2/\sqrt{3}$ as determined by the von Mises yield criterion is adopted in present analyses and provides an upper bound (conservative) estimate for the failure pressure of a defect-free pipe. To further explore the significance of the adopted failure stress criterion, the analyses consider plastic instability of the ligament defined by $\sigma_e \geq \eta \sigma_u$ where η takes the values 0.8, 0.9 and 1.0.

Not surprisingly, there is a negligible effect of defect width for both defect shapes on the normalized failure pressure for all adopted η-values. The results for the groove-shaped defect displayed in Fig. 6(a-b) reveal a slight elevation in failure pressure for $d_g = 0.2$ mm which is most likely associated with the development of plasticity and strong stress gradients due to the very narrow groove size adopted. Following this short "transient", however, the failure pressure remains essentially constant over the entire range of groove size. The results plotted in Fig. 7 for the rectangular-shaped defect also show virtually no effect of defect width on the normalized pressure. Note, however, a slight decrease in the failure pressure for both deep and shallow flaw when compared with corresponding failure pressures for the groove-shaped defect.
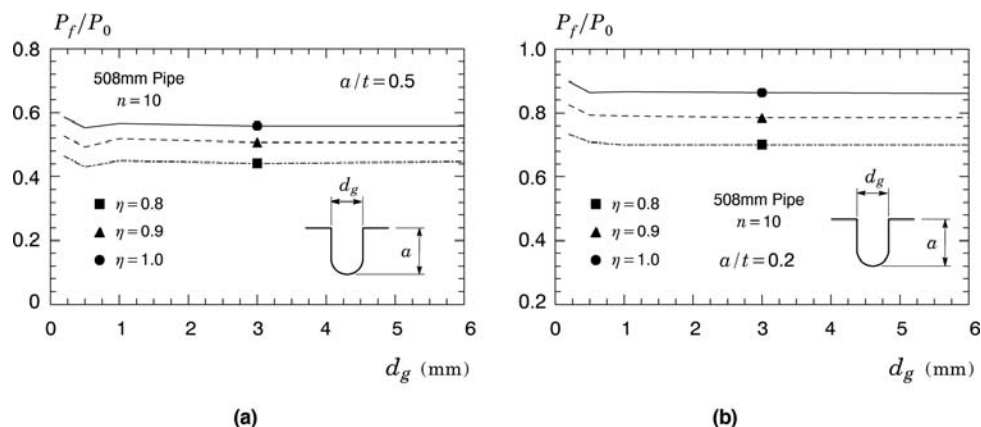
Figure 6. Dependence of normalized failure pressure on defect width for the $n = 10$ pipe with groove-shaped defect and varying η-parameters. (a) $a/t = 0.5$; (b) $a/t = 0.2$.
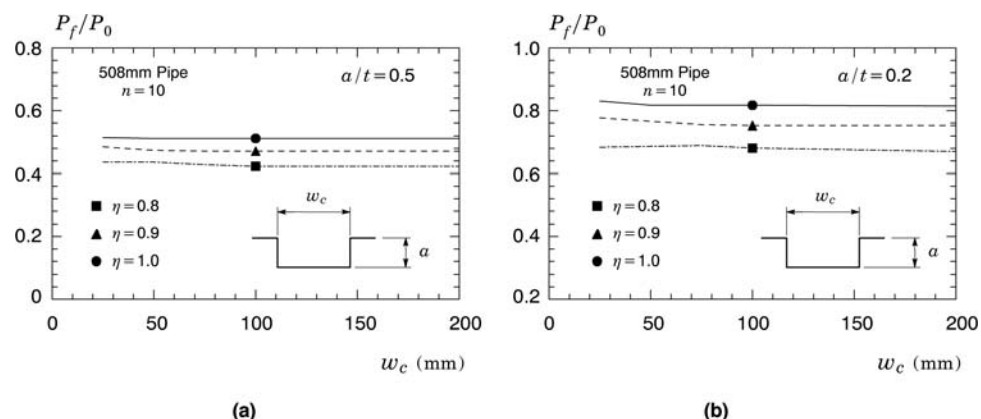

Figure 7. Dependence of normalized failure pressure on defect width for the $n = 10$ pipe with rectangular-shaped defect and varying η-parameters. (a) $a/t = 0.5$; (b) $a/t = 0.2$.

4. APPLICATION TO BURST PRESSURE TESTING OF CORRODED PIPES

4.1. API X65 Pipe Specimens

The burst pressure prediction for the pipe specimens with external defects tested by Kim et al. (2004) follows limit load analyses based on the evolution of von Mises stress contours along the remaining ligament outlined in Section 3. The integrity analyses presented here compare the predicted burst pressure, hereafter denoted P_{f-pred}, associated with the plastic instability of the remaining ligament and defined through $\sigma_e = \eta \sigma_u$, where η takes the values 0.8, 0.85, 0.9, and 1.0, for the 3-D models described in Section 2.2. Figure 8(a) shows the predicted burst pressure for the analyzed pipes based on plastic instability of the remaining ligament defined through $\sigma_e = \eta \sigma_u$ for different η values. The solid symbols in the figure represent predicted values while the solid line defines the equality between predicted and experimental values, i.e., $P_{f-exp} = P_{f-pred}$. The burst pressures predicted by ASME B31.G (ASME, 1991) and DNV RP-F101 (DNV, 2004) are also plotted in the figure and, in this case, the predicted values are represented by open symbols. To facilitate the interpretation of the defect length effect on the predicted burst pressure, the arrow in Figure 8(a) shows increased burst pressure with decreased defect length.

These results clearly reveal the strong effect of η values on the predicted burst pressure based on plastic instability of the remaining ligament. For $\eta = 1.0$, the analyses consistently overestimate by approximately 15% the burst pressure for almost all range of defect length; in this case, only the burst pressure predicted for the pipe specimen with defect length $2c = 50$ mm is below the experimental burst pressure. By contrast, all the analyses with $\eta = 0.8$ underestimate the burst pressure for all defect lengths; here, a more significant deviation from experimental results is observed for

short defects ($2c = 200 \sim 300$ mm). Burst predictions provided by $\eta = 0.9$ provides better agreement with experimental data, although the analyses also overestimate the predicted burst pressure by $\approx 5\%$; once again, only the burst pressure predicted for the shortest defect ($2c = 50$ mm) is slightly underestimated. Moreover, in accordance with previous studies, predictions based on ASME B31.G (ASME, 1991) and DNV RP-F101 (DNV, 2004) procedures provide large margins between experimental and predicted values, particularly for the ASME methodology.
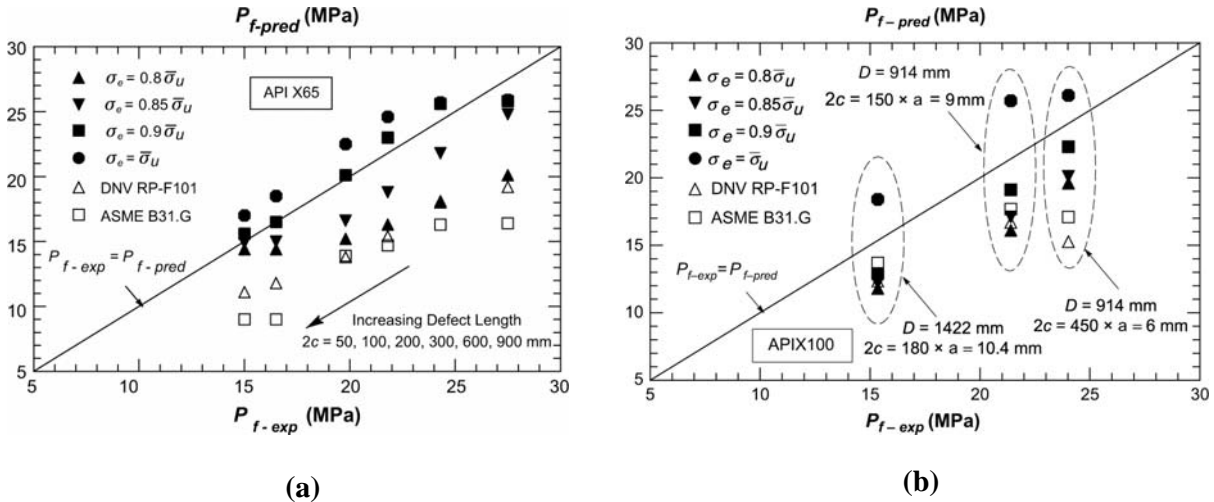

(a)   **(b)**

Figure 8. Comparison between experimental and predicted burst pressure (a) API X65 specimens (b) API X100 specimens.

4.2. API X100 Pipe Specimens

The burst pressure prediction for the tested pipe specimens made of API X100 steel described in section 2.2. follows the same methodology presented previously which is based on the plastic instability of the remaining ligament defined through $\sigma_e \geq \eta \sigma_u$. Figure 8(b) shows predicted burst pressure for the analyzed pipes based on plastic instability of the remaining ligament for different η values. The solid symbols in the figure represent predicted values while the solid line defines the equality between predicted and experimental values, i.e., $P_{f-\exp} = P_{f-pred}$. The burst pressures predicted by ASME B31.G (ASME, 1991) and DNV RP-F101 (DNV, 2004) are also plotted in the figure and, in this case, the predicted values are represented by open symbols.

In contrast with the results presented for API X65, the burst predictions for API X100 pipe specimens exhibit a weaker dependence of η factor. Here, excepting for $\eta = 1.0$ all the burst predictions are below the line $P_{f-\exp} = P_{f-pred}$ and provide better agreement between predictions and experimental results for $\eta = 0.9$. Further, results provided by ASME B31.G (ASME, 1991) and DNV RP-F101 (DNV, 2004) reveal a mixed behavior. While for $D = 914$ mm it exhibits large margins in comparison with experimental tests, especially for $2c = 450 \times a = 6$ mm, it shows better agreement for $D = 1422$ mm.

5. COMPARISON WITH LIMIT LOAD SOLUTION FOR CORROSION DEFECT ASSESSMENT

The procedure presented here to predict the burst pressure of corroded pipes relies rather heavily on detailed, nonlinear finite element analyses. In this section we compare the experimental results of API X65 and X100 pipe specimens showed previously with the solution proposed by Choi et al. (2003). This solution is adopted due to its relative simplicity and rather extensive calibration derived from numerical analyses conducted on models for thin-walled corroded pipes with varying D/t ratio and defect geometry.

Figure 9(a-b) shows the burst pressure predicted by Choi's solutions for the analyzed API X65 and X100 pipe specimens. The solid line in both figures defines the equality between predicted and experimental values. Focusing attention on API X65 results, it can be observed in Figure 9(a) a general good agreement between experimental and predicted values. For this set of defect length, the burst pressure predicted by Choi slightly overestimates the experimental results for short defects ($2c = 50$ and 100 mm); while for long defects it underestimates ($2c = 900$ mm). Now, direct attention to the API X100 results (Figure 9(b)). Apart from $D = 914$ mm and $2c = 450 \times a = 6$ mm pipe specimen, all the burst pressure were overestimated by Choi's solution by a factor of ~10%. Since the limit load

solution provided by Choi et al. (2003) is also based upon the criterion $\sigma_e \geq \eta\sigma_u$ with $\eta = 0.9$, these analyses, albeit rather limited, further indicate the potential dependence of a ''correct'' choice for the η value upon defect geometry and strain hardening behavior.
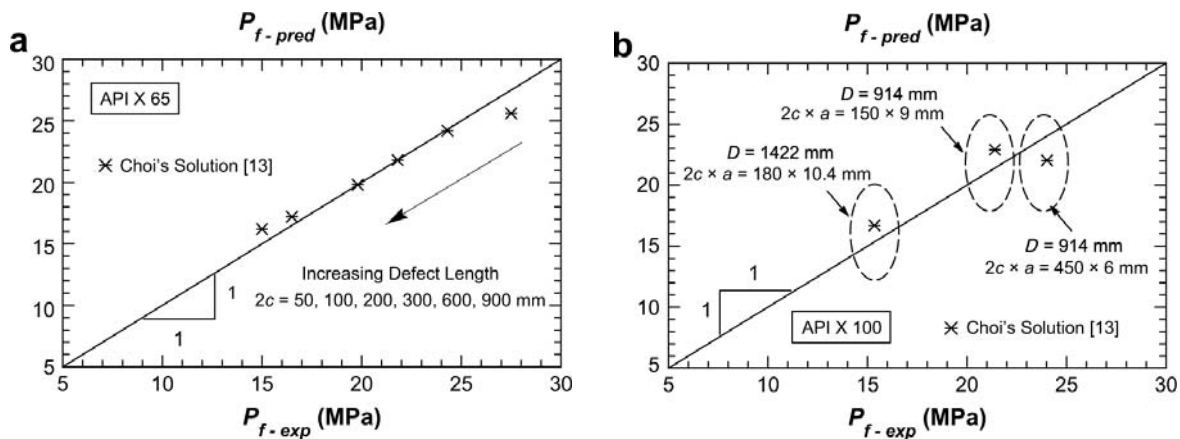

Figure 9. Comparison between Choi's limit load solution (Choi et al., 2003) and experimental burst pressure (a) API X65 specimens (b) API X100 specimens.

6. DISCUSSIONS AND CONCLUDING REMARKS

The parametric analyses of local ligament instability for flawed pipes described here, coupled with the exploratory study to predict experimentally measured burst pressure provides a rational basis for the use of stress based criterion in corroded pipe assessments. The analyses consider a failure criterion based on the evolution of high stress contours over the remaining ligament up to the achievement of a local limit load. In the methodology adopted in the present work, such criterion becomes a simple description of the remaining ligament instability defined as $\sigma_e \geq \eta\sigma_u$, where η takes the values 0.8, 0.85, 0.9, and 1.0.

Extensive plane-strain analyses conducted on pipe models with axial flaws demonstrate the independence of the ligament instability criterion on key geometrical and material parameters controlling the failure pressure, including defect shape (groove *vs.* rectangle), and defect width. A central result derived from these analyses is that burst pressure defined by attainment of plastic instability of defect ligament displays very weak sensitivity on defect shape even though the contour maps for which $\sigma_e \geq \sigma_u$ differ significantly for groove and rectangular-shaped defects. This conclusion suggests that the computational demands to accurately model the correct defect shape can be minimized while maintaining an adequate resolution of ligament stresses.

A validation study employed experimentally measured burst pressure data of pipe specimens made of API X65 and X100 steels to demonstrate the capability of a stress based criterion, defined in terms of remaining ligament instability, to predict the burst pressure of the tested pipes. Although the analyses showed the effectiveness of such criterion based on $\sigma_e \geq \eta\sigma_u$ in burst pressure predictions, the η factor exhibits a potential strong dependence on the defect geometry and material properties. This characteristic can adversely affect burst predictions and potentially prevent the use of a "correct" safety margin due to the mixed tendency of conservatism/pessimism observed for both materials (API X65 and X100). Further verification studies based upon a recently proposed limit load solution (Choi et al., 2003) most applicable to thin-walled corroded pipelines also confirm these observed trends. Such conclusions can also lead to some concerns about the applicability of actual limit load solutions for pipes with axial flaws and corrosion defects incorporated in current defect assessment procedures such as API 579 (API, 2007) and SINTAP (SINTAP, 1999). Although the necessity of additional numerical analyses and experimental results to precisely evaluate the effect of defect geometry and material properties on η factor, the results presented here provide a strong support to the use of stress based approaches incorporating instability analyses of the remaining ligament in defect assessment of corroded pipes.

6. ACKNOWLEDGEMENTS

7. REFERENCES

AMERICAN PETROLEUM INSTITUTE, Fitness-for-Service, API RP-579-1 / ASME FFS-1, 2007.

AMERICAN SOCIETY OF MECHANICAL ENGINEERS. Manual for Determining the Remaining Strength of Corroded Pipelines - ASME B31G, Three Park Avenue, NewYork, 1991.

ANDERSON, T. L.. Fracture Mechanics: Fundaments and Applications - 3rd Edition, CRC Press, New York, 2005.

BATTE, A. D., FU, B., KIRKWOOD, M. G. AND VU, D.. New Methods for Determining the Remaining Strength of Corroded Pipelines, in: *Offshore Mechanics and Arctic Engineering Conference (OMAE)*, Vol. V, pp. 221-228 (Pipeline Technology), 1997.

CHAKRABARTY, J., Theory of Plasticity - 3rd Edition, Elsevier B. V., Oxford, 2006.

CHIODO, M. S. G. AND RUGGIERI, C.. Failure Assessments of Corroded Pipelines with Axial Defects Using Stress-Based Criteria: Numerical Studies and Verification Analyses", *International Journal of Pressure Vessels and Piping*, Vol. 86, pp. 164-176, 2009.

CHOI, J. B., GOO, B. K., KIM, J. C., KIM, Y. J. AND KIM,W. S.. Development of Limit Load Solutions for Corroded Gas Pipelines, *International Journal of Pressure Vessels and Piping*, Vol. 80, pp. 121-128, 2003.

CRAVERO, S. AND RUGGIERI, C., "Correlation of Fracture Behavior in High Pressure Pipelines with Axial Flaws Using Constraint Designed Test Specimens - Part I: Plane-Strain Analyses," Engineering Fracture Mechanics, Vol. 72, pp. 1344-1360, 2005.

DET NORSK VERITAS. Corroded Pipelines, *DNV-RP-F101*, 2004.

DOTTA, F. AND RUGGIERI, C., "Structural Integrity Assessments of High Pressure Pipelines with Axial Flaws Using a Micromechanics Model, *International Journal of Pressure Vessels and Piping*, Vol. 81, pp. 761-770, 2004.

EIBER, R. J. AND KIEFNER, J. F. Failure of Pipelines, in: *Metals Handbook*, Ninth Edition, Vol. 11 - Failure Analysis and Prevention, American Society for Metals, pp. 695-706, 1986.

FU, B. AND KIRKWOOD, M. G.. Determination of Failure Pressure of Corroded Linepipes Using the Nonlinear Finite Element Method, *Proceedings of the 2nd Intl. Pipeline Technology Conference*, Vol. II, pp. 1-9, 1995.

KARSTENSEN, A., SMITH, A.AND SMITH, S.. Corrosion Damage Assessment and Burst Test Validation of 8in X52 Linepipe, *Pressure Vessel Piping Design Analysis*, Vol. 430, pp. 189-194, 2001.

KIEFNER, J. F. AND VIETH, P. H.. A Modified Criterion for Evaluating the Remaining Strength of Corroded Pipe, Final Report on *Project PR 3-805*, Pipeline Research Committee, American Gas Association, Batelle, Ohio, 1989.

KIEFNER, J. F., MAXEY, W. A., EIBER, R. J. AND DUFFY, A. R.. Failure Stress Levels of Flaws in Pressurized Cylinders, in: *Progress in Flaw Growth and Fracture Toughness Testing*, ASTM STP 536, pp. 461-481, American Society for Testing and Materials, Philadelphia, 1973.

KIM,Y.P.,KIM,W. S., LEE,Y.K.ANDOH, K.H.. The Evaluation of Failure Pressure for Corrosion Defects within Girth or Seam Weld in Transmission Pipelines, in: *International Pipeline Conference (IPC)*, Calgary, Alberta, Canada, 2004.

KOPPENHOEFER, K., GULLERUD, A., RUGGIERI, C., DODDS, R. E HEALY, B.. WARP3D: Dynamic Nonlinear Analysis of Solids Using a Preconditioned Conjugate Gradient Software Architecture, *Structural Research Series (SRS) 596*. UILU-ENG-94-2017. University of Illinois at Urbana-Champaign, 1994.

LEIS, B. N.ANDSTEPHENS, D. R.. An Alternative Approach to Assess the Integrity of Corroded Line Pipe − Part I: Current Status, in: *International Offshore and Polar Engineering Conference (ISOPE)*, Vol. IV, pp. 624-634, 1997.

MAES, M. A., SALAMA, M. M. E DANN M.. Reliability of Burst Limit States for Damaged and Corroded High Strength Pipeline, in: *25th Offshore Mechanics and Arctic Engineering Conference (OMAE)*, 2006.

MANNUCCI, G., DEMOFONTI, G., BARSANTI, L., HARRIS, D. AND HILLENBRAND, H. G.. Fracture Properties of API X100 Gas Pipeline Steels, in: *13th Biennial EPRG-PRCI Joint Technical Meeting*, New Orleans, Louisiana, USA, 2001.

NORONHA, D. B., BENJAMIN, A. C. AND ANDRADE, E. Q.. Finite Element Models for the Prediction of the Failure Pressure of Pipelines with Long Corrosion Defects, in: *International Pipeline Conference (IPC)*, Calgary, Alberta, Canada, 2002.

SINTAP: Structural Integrity Assessment Procedure for European Industry. Final Procedure, 1999.

STAAT,M.. Local and Global Collapse Pressure of Longitudinally Flawed Pipes and Cylindrical Vessels, International Journal of Pressure Vessels and Piping, Vol. 82, pp. 217-225, 2005.

STAAT, M.. Plastic Collapse Analysis of Longitudinally Flawed Pipes and Vessels, *Nuclear Engineering and Design*, Vol. 234, pp. 25-43, 2004.

STAAT, M. AND VU,D. K.. Limit Analysis of Flaws in Pressurized Pipes and Cylindrical Vessels. Part I: Axial Defects, *Engineering Fracture Mechanics*, Vol. 74, pp. 431-450, 2007.

SILVA, L. A. L., CRAVERO, S. AND RUGGIERI, C., "Correlation of Fracture Behavior in High Pressure Pipelines with Axial Flaws Using Constraint Designed Test Specimens - Part II: 3-D Effects on Constraint," Engineering Fracture Mechanics, Vol. 73, pp. 2123-2138, 2006.

WILKOWSKI, G., STEPHENS, G. KRISHNASWAMY, P., LEIS, B. AND RUDLAND, D.. Progress in Development of Acceptance Criteria for Local Thinned Areas in Pipe and Piping Components, *Nuclear Engineering and Design*, Vol. 195, pp. 149-169, 2000.

ZHU, X. K. AND LEIS, B. N.. Theoretical and Numerical Predictions of BurstPressure of Pipelines, in: *ASME Pressure Vessels and Piping Division Conference (PVP)*, Vancouver, BC, Canada, 2005.

8. RESPONSIBILITY NOTICE

The authors are the only responsible for the printed material included in this paper.